# Molecular Dynamics Simulations of Graphene Oxide Frameworks

Adrien Nicolaï,[†] Pan Zhu,[†] Bobby G. Sumpter,[‡] and Vincent Meunier*,[†]

[†]Department of Physics, Applied Physics and Astronomy, Rensselaer Polytechnic Institute, Troy, New York 12180, United States

[‡]Center for Nanophase Materials Science and Computer Science and Mathematics Division, Oak Ridge National Laboratory, Oak Ridge, Tennessee 37831, United States

ABSTRACT: We use quantum mechanical calculations to develop a full set of force field parameters in order to perform molecular dynamics simulations to understand and optimize the molecular storage properties inside graphene oxide frameworks (GOFs). A set of boron-related parameters for commonly used empirical force fields is determined to describe the nonbonded and bonded interactions between linear boronic acid linkers and graphene sheets of GOF materials. The transferability of the parameters is discussed and their validity is quantified by comparing quantum mechanical and molecular mechanical structural and vibrational properties. The application of the model to the dynamics of water inside the GOFs reveals significant variations in structural flexibility depending on the linker density, which is shown to be usable as a tuning parameter for desired diffusion properties.
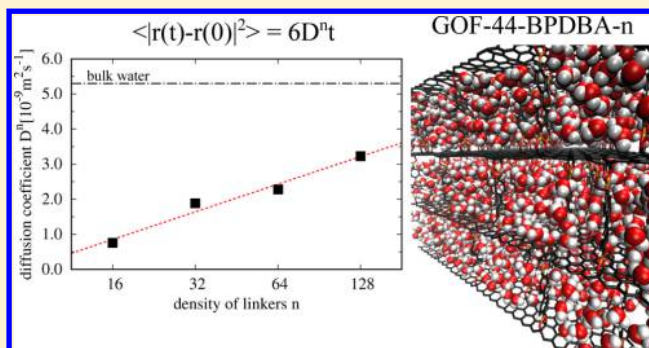
INTRODUCTION

Graphene oxide framework (GOF) materials are a class of porous materials consisting of layers of graphene oxide (GO) sheets interconnected by linear boronic acid pillaring units, also called linkers.[1] GOF materials were synthesized in 2011 through boronate—ester formation as a result of B—O bonding between boronic acids and oxygen functional groups on the GO layers.[2] The synthesis of GOF materials has generated tremendous interest for energy related applications. In that context, several experimental studies have been performed to investigate the chemical tunability and potential for energy-related applications. For instance, it has been shown experimentally that with proper choice of pillaring unit size and concentration,[1] GOF materials with large pore size, pore volume, and high accessible surface area are promising candidates for gas storage, catalytic support, and energy storage.[1−3]

Computer simulations are a powerful tool for complementing experiments to gain atomistic understanding of GOF material properties. First-principles calculations of the electronic and thermal properties of GOF materials based on density functional theory (DFT) were recently performed to demonstrate that GOF materials have tunable electronic properties depending on linker composition and density.[4] However, there have been no studies concerning the dynamical properties of GOF materials and their flexibility in a solvated environment. To-date, such molecular dynamics (MD) simulations have been hindered by the lack of molecular mechanics (MM) parameters for linear boronic acid compounds.

In the present work, we consider idealized GOF-L-n materials (Figure 1A), where L stands for 4,4′-biphenyldiboronic acid linker (L = 44BPDBA) and n stands for the number of carbon atom on graphene per linker. In this notation a large value for n corresponds to a low density of linkers $1/n$. Force field parameters essential to the description of phenylboronic
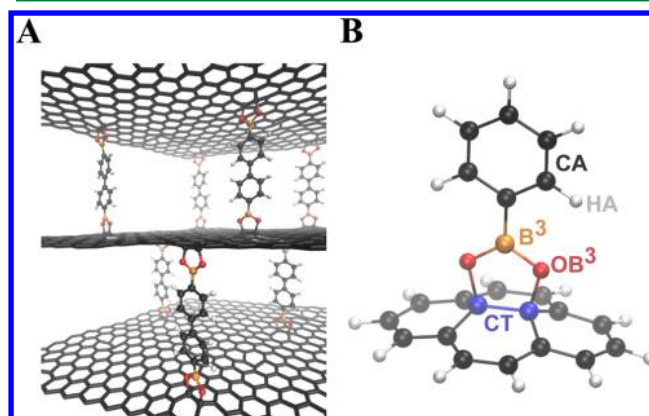
Figure 1. [A] All-atom three-dimensional structure of GOF-44BPDBA-128. [B] All-atom three-dimensional structure of the chosen PBA model fragment used in force field parametrization with atom types indicated (see Table 1 for details). For all the atomic structures shown in the present paper, carbon atoms are shown in black (CT atoms are shown in blue for this panel only), boron atoms in orange, oxygen atoms in red, and hydrogen atoms in white.

acid (PBA) related linkers are missing in the literature, which precludes the dynamical studies of GOF-L materials in realistic environments. This is specifically the case for trigonal planar boron atoms (B^3) and oxygen atoms bonded to boron atoms (OB^3, Table 1), even though boron-related parameters were

Table 1. Atom Type Assignment

type	description
CA	aromatic carbon
HA	aromatic hydrogen
B^3	boron trigonal planar
OB^3	oxygen bound to trigonal boron and aliphatic carbon
CT	aliphatic carbon (sp^3)

introduced in some of the most popular force fields such as AMBER,[5] CHARMM,[6] or OPLS.[7] It is generally assumed that MM parameters may be transferred to larger systems, composed of the same atoms or bonds. Unfortunately, the above parameters[5–7] are molecule dependent and are not directly transferable to 44BPDBA linkers. Therefore, new parameters for these two types of atoms need to be determined before an accurate study of the dynamical properties of GOFs can be performed.

Here, we present a MM force field parametrization for a PBA model fragment, shown in Figure 1B and based on the AMBER empirical force field[8] potential energy surface. The bonded interactions were parametrized by computing quantum mechanical (QM) energy profiles from ab initio calculations and by fitting the corresponding QM energy profiles with analytical functions defining the potential energy surface of the AMBER force field.[8] In addition, the electrostatic interactions have been derived from the QM electrostatic potential fitting method (RESP).[9] Care was taken to ensure a total zero charge of the system and to properly transfer the parametrized partial atomic charges from the chosen PBA model fragment to GOF materials. The new parameters were then used in the existing AMBER-99 force field[10] and validated by comparing QM and MM structural and vibrational properties. The satisfactory agreement between QM and MM properties suggests the transferability and suitability of the present parameters for use in MD simulations of GOF materials. Using this parametrization, MD simulations of GOF-L-n materials were performed using the GROMACS software package[11] in explicit water and for varying linker densities.

■ MATERIALS AND METHODS

Force Field Parameterization. *Parameterization Procedure.* The AMBER force field[8] is an empirical force field and is defined by a potential energy surface V, modeled as the sum of bonded (V_{bonded}) and nonbonded ($V_{non-bonded}$) interactions. The former is represented by contributions from covalent bond stretching, angle bending, and torsion:

$$V_{bonded} = \sum_{bonds} K_b(b - b_0)^2 + \sum_{angles} K_\theta(\theta - \theta_0)^2 + \sum_{torsions} \frac{K_\phi}{2}(1 + \cos[m\phi - \psi])$$

(1)

where b_0 and θ_0 are the equilibrium bond lengths and bond angles; ϕ and ψ are the torsion and the phase angles; m is the multiplicity of the periodic torsion angle potential; and K_b, K_θ, and K_ϕ are the bond stretching, bending, and torsion angle

force constants. The nonbonded interactions account for the van der Waals (vdW) and electrostatic terms, i.e., Lennard-Jones and Coulomb potentials, respectively:

$$V_{non-bonded} = \sum_i \sum_{j \neq i} 4\varepsilon_{ij}\left[\left(\frac{\sigma_{ij}}{r_{ij}}\right)^{12} - \left(\frac{\sigma_{ij}}{r_{ij}}\right)^6\right] + \frac{q_i q_j}{4\pi\varepsilon_0 r_{ij}}$$

(2)

where r_{ij} is the distance between atoms i and j; σ_{ij} and ε_{ij} are Lennard-Jones parameters for atom pair $i-j$; q_i is the partial atomic charge q of atom i; and ε_0 is the dielectric permittivity of vacuum. Note that vdW interactions are expressed by the same rules employed by the empirical AMBER force field,[8] i.e., $\varepsilon_{ij} = (\varepsilon_i \varepsilon_j)^{1/2}$ and $\sigma_{ij} = 1/2(\sigma_i + \sigma_j)$.

The goal of a parametrization is to provide accurate estimates for b_0, θ_0, ψ, m, K, q_i, σ_i, and ε_i, for all the interactions between the atom types involved in the system. These parameters can be either obtained from experimental and/or quantum mechanical calculations of small molecules or representative molecular fragments. Here, the force field parameters for trigonal planar boron atoms and oxygen atoms bonded to boron atoms were obtained by considering two factors. First, MM energy profiles defined by the potential energy surface in eqs 1 and 2 were computed to accurately reproduce QM energy profiles. Second, compatibility with the existing AMBER-99 force field[8,10] was enforced by restricting the calculations to parameters that did not already exist in this force field.

A PBA model fragment was used to make the parametrization computationally tractable (Figure 1B), since extensive QM calculations on a full GOF structure (Figure 1A) are technically precluded. The specific PBA fragment was chosen to preserve the same chemical environment for each atom type of PBA-based linkers, compared to a full GOF structure (Figure 1). The corresponding PBA model fragment (Figure 1B) is made up of a PBA molecule attached to four carbon hexagonal rings, used to model a graphene sheet. The edges were passivated with hydrogen. The symmetry of the chosen PBA model fragment corresponds to point group C_{2v}.

Computational Details. All QM calculations were performed with the NWChem 6.1 package.[12] Geometry optimizations are based on DFT calculations at the hybrid B3LYP[13,14] level of theory using the cc-pVDZ basis set.[15] The DRIVER module of NWChem was used for geometry optimization, which is a quasi-Newton optimization with line searches and approximate energy Hessian updates.

Bonded Parameters. To obtain force constants K_b, K_θ, and K_ϕ, we computed QM energy profiles for each bond length b, bond angle θ, and torsion angle ϕ by varying these geometric parameters to reproduce the shape of their potential energy functions (i.e., harmonic for the bond lengths and bond angles and periodic for the torsion angles). Appropriate constraints were imposed during geometry optimization to keep the internal coordinate of interest constant, while the remaining degrees of freedom were allowed to relax to an energy minimum corresponding to the constraint. QM energy profiles of bond lengths were obtained by scanning the selected bond length from its equilibrium value b_0 to $b_0 \pm 0.005$ nm by steps of 0.001 nm. QM energy profiles of bond angles were obtained by scanning the selected bond angle from its equilibrium value θ_0 to $\theta_0 \pm 5°$ by steps of 1°. Finally, QM energy profiles of torsion angles were obtained by scanning their complete range of possible values, i.e., from 0 to 360° by steps of 10°. For the MM torsion angle energy profiles, the energy of a conformer

was minimized using the conugate gradient algorithm, in which the selected torsion angle was held constant using MM restraints as implemented in GROMACS,[16] while the remaining degrees of freedom were allowed to relax.

Nonbonded Parameters. Partial atomic charges q (eq 2) were obtained from a restricted fit to the QM electrostatic potential, also known as the RESP method.[9] RESP fits charges to reproduce QM electrostatic potential calculated on selected grid points. The level of theory used for this calculation is the same as that used for geometry optimization. Compared to the PBA model fragment used for geometry optimization (Figure 1B), we increased the number of hexagonal rings from 4 to 30 to represent the graphene sheet (inset in Figure 2A), to avoid
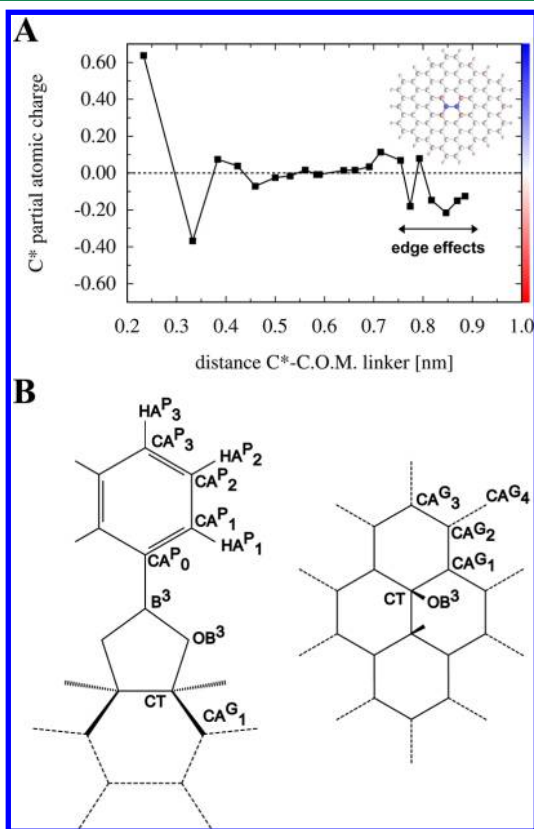
Figure 2. [A] Partial atomic charges q ($|e|$ unit) of carbon atoms C* belonging to the graphene sheet (see inset) as function of the distance between these C* atoms and the center of mass (C.O.M.) of the PBA linker. [B] Sketches of the model fragment used in parametrization of partial atomic charges with atom names indicated.

spurious edge effects in the calculation of partial atomic charges. Lennard-Jones parameters σ and ε (eq 2) for B[3] and OB[3] atom types, which were missing in the AMBER-99 force field,[10] were adopted from a previous work[6] based on the ab initio studies of model enolborane systems. Note that these LJ parameters[6] have already been used in a previous work for force field implementation of boron-related compounds.[5] The numerical values for these parameters are $\sigma = 3.53 \times 10^{-1}$ and 2.85×10^{-1} nm and $\varepsilon = 1.42 \times 10^{-1}$ and 6.66×10^{-1} kJ/mol for B[3] and OB[3] atoms, respectively. The LJ parameters for the other atom types defined in Table 1 were adopted from the existing AMBER-99 force field.[10]

Molecular Dynamics Simulations. All MM calculations and MD simulations have been carried out with the GROMACS 4.5.5 software package,[16] using the AMBER-99 force field[10]

including the new parameters for B[3] and OB[3] atom types developed in the present work. MM energy minimizations of GOF structures in vacuum and in an aqueous environment were performed using the conjugate gradient algorithm.[16] MD simulations of GOF materials filled with water molecules were carried out using the TIP3P model of water.[17] The time step used in all simulations was 1 fs, and the neighbor list was updated every step with the grid method[16] and a cutoff radius of 1 nm. The coordinates of all the atoms in the simulation box were saved every 100 fs. The initial velocities were chosen randomly. We used the NPT ensemble with a hexagonal box. The dimensions of the simulation box, the number of GOF atoms and water molecules and the water density for each GOF-L-*n* material studied are provided in Table 2.

Table 2. Details of GOF Materials Simulated by MD in the Present Work[a]

n	number of GOF atoms	simulation box [nm³]	number of water molecule
∞	1024 (0)	3.94 × 3.40 × 3.12	925
128	1232 (8)	3.94 × 3.40 × 3.12	841
64	1440 (16)	3.94 × 3.40 × 3.12	757
32	1856 (32)	3.94 × 3.40 × 3.12	610
16	2688 (64)	3.88 × 3.38 × 3.21	355

[a]The number between the parentheses indicates the number of linkers per simulation box.

The temperature and pressure were kept at desired values using the Nosé−Hoover thermostat[18,19] ($T = 300$ K, $\tau_T = 0.1$ ps) and an isotropic coupling for the pressure from a Parinello−Rahman barostat[20] ($P_0 = 1$ bar, $\chi = 4.5 \times 10^{-5}$ bar^{-1}, $\tau_P = 2.0$ ps). The electrostatic term was computed using the particle mesh Ewald (PME) algorithm[21] (with a radius of 1 nm) with the fast Fourier transform optimization (with an order equal to 4 for the interpolation). The cutoff algorithm[16] was applied for the non-Coulomb potentials with a radius of 1 nm. The system was initially heated for 50 ps and equilibrated for 500 ps with lower restraints for atom positions and LINCS[22] constraints for all bonds, finishing with no restraints and constraints at 300 K. MD runs of 20 ns for each GOF-L-*n* material were performed. We also performed a MD run of TIP3P bulk water using the same parameters for comparison.

■ RESULTS AND DISCUSSION

Force Field Parameterization of PBA Model Fragment. *Partial Atomic Charges.* Partial atomic charges q for the PBA linker and the hexagonal carbon rings composing the chosen PBA model fragment (Figure 1B) were derived by applying the RESP method.[9] The full list of RESP charges obtained is shown in Table 3. It is generally assumed that, for graphene materials, partial atomic charges of aromatic carbon atoms are null due to the symmetry of the system. In the case of GOF materials, we relaxed this assumption and computed the partial atomic charges of carbon atoms C* belonging to the graphene sheet (C* for CA or CT), as a function of the distance from each C* atom to the center of mass (C.O.M.) of the PBA linker. This procedure was devised in order to establish the influence of a PBA linker in the partial atomic charges of C* atoms of the graphene sheet (Figure 2A). As shown in Figure 2A, CT atoms have a significant positive charge, $q = +0.637|e|$ (at a distance equal to 0.16 nm). In addition, the first four aromatic carbon atoms of the graphene

Table 3. Atom Names and Partial Atomic Charges q (|e| unit) Computed from the RESP Method before and after Refinement (See Text)[a]

atom name	RESP charges	adjusted charges
CA^P_0	−0.085	−0.085
CA^P_1	−0.034	−0.025
CA^P_2	−0.079	−0.070
CA^P_3	−0.098	−0.089
HA^P_1	0.067	0.076
HA^P_2	0.057	0.066
HA^P_3	0.084	0.000
B^3	0.324	0.324
OB^3	−0.377	−0.377
CT	0.637	0.755
CA^G_1	−0.368	−0.250
$CA^G_{n \geq 2}$	∼0.000	0.000

[a]P or G superscript indices correspond to aromatic carbon atoms which belong to the phenyl ring and to the graphene sheet, respectively. Atom names refer to Figure 2B.

sheet bound to CT atoms (at a distance equal to 0.23 nm), named CA^G_1, have a significant negative charge, i.e., $q = -0.368|e|$ (Table 3). The other CA^G_i atoms (Figure 2A), for $2 \leq i \leq n$ where n is the number of graphene carbons per linker unit (GOF-L-n), have only residual charges close to $q = 0$, except for CA^G atoms which are influenced by the edge effects of hydrogen atoms (HA^G) of the graphene sheet (distance >0.7 nm, Figure 2A).

Adjustments to the RESP charges were required to guarantee their transferability to the GOF-L-n materials. First, to avoid edge effects observed for the graphene sheet due to the presence of H atoms, we imposed the HA^G and CA^G atoms bound to HA^G atoms to be charge neutral. To keep a total zero charge for the entire system, we distributed their initial RESP charges to all the other carbon atoms of the graphene sheet. Second, since one of the main goals of this work is to study the effect of linker density $1/n$ on the structural and dynamical properties of GOF materials ($n = 16, 32, 64,$ and 128), we set to $q = 0$ all the charges of the CA^G_i atoms (Figure 2 B), $2 \leq i \leq n$, in agreement with the residual charges of these atoms (which were found to be very close to zero, Figure 2A) calculated with the RESP method (Figure 2B). As done previously for HA^G and CA^G atoms of the edges, these residual charges were distributed equally to the remaining atoms of the graphene sheet, i.e., CT and CA^G_1.

Finally, as shown in Figure 1, accurate calculations must account for the difference between the actual linkers of GOF materials (44BPDBA) and the chosen PBA model fragment. Specifically, the difference consists of the presence of HA^P_3 in the chosen PBA model fragment. In 44BPDBA linkers of the GOF materials, this atom is substituted by a CA^P_3, which belongs to the second PBA. Therefore we set the partial atomic charge of HA^P_3 atom $q = 0$ and distribute the RESP charge to the other atoms CA^P and HA^P of the phenyl ring, allowing us to keep a total neutrality for the entire fragment. Given the above considerations, the partial atomic charges of HA^P, CA^P, CA^G, and CT atoms were adjusted compared to the initial RESP charges in order to, first, ensure their transferability to GOF materials and, second, to keep a zero total charge for all the different GOF-L-n. The partial atomic charges q added in the AMBER-99 force field for the chosen PBA model fragment are given in Table 3.

Bond Length Parameters. B^3 and OB^3 atoms, for which there is no parameters in the current AMBER-99 force field,[10] are involved in three different bonds of the chosen PBA model fragment: CA−B^3, B^3−OB^3, and OB^3−CT. The equilibrium values of these bond lengths were obtained by QM geometry optimization of the PBA model fragment (Figure 3) and are listed in Table 4.
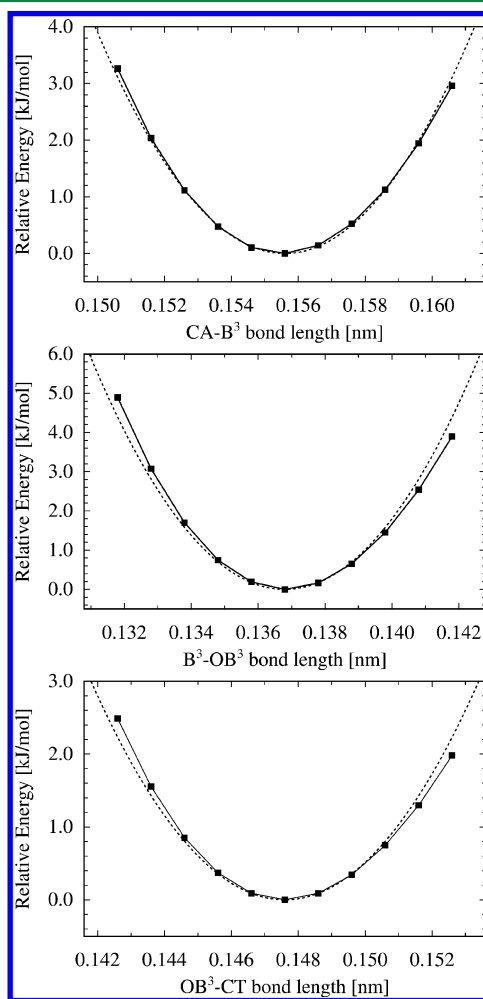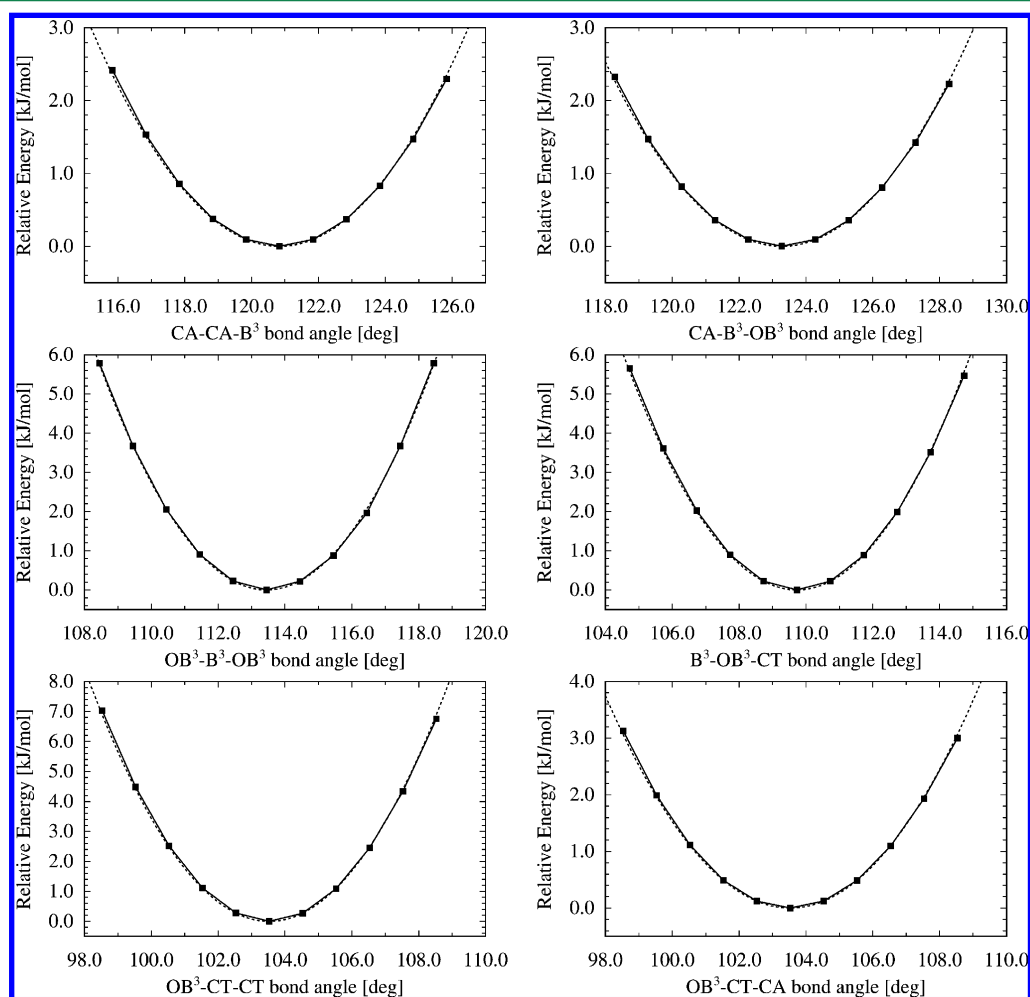

Figure 3. QM energy profiles (solid lines) for bond lengths CA−B^3, B^3−OB^3, and OB^3−CT. Dashed lines represent the fit of the QM data by an harmonic potential as described in eq 1

To compare the computed values with experimental data, a search of crystal structures containing PBA functions should be performed among available crystal structure databases. This search was completed by Otkidach and Pletnev[6] on the Cambridge Crystal Structure Database (CSD).[23] The closest crystal structure containing a PBA group is the structure referred by its CSD name *MANBOS*. The calculated values of the bond lengths agreed very well with the experimental values (cf. Table 4): CA−B^3(0.156 nm) and B^3−OB^3(0.137 nm). Further, the force constants K_b associated with the bond lengths mentioned above were obtained by fitting a harmonic potential on the QM energy profiles (Figure 3). The relevance of this method is justified by the agreement between analytical and computational energy profiles (see Figure 3).

Bond Angle Parameters. The same procedure employed for bond length parameters was followed to obtain bond angle parameters (Figure 4).

Table 4. Force Field Bonded Parameters for the PBA Model Fragment Obtained from ab initio Calculations[a]

bond length	eq bond length b_0 [nm]	exp X-ray data [nm]	force constant K_b [kJ/mol·nm²]
CA–B³	0.1556	0.156	248.9×10^3
B³–OB³	0.1368	0.137	351.4×10^3
OB³–CT	0.1476		178.6×10^3
bond angle	**eq bond angle θ_0 [deg]**	**exp X-ray data [deg]**	**force constant [kJ/mol·rad²]**
CA–CA–B³	120.8		618.2
CA–B³–OB³	123.3	123.0	596.6
OB³–B³–OB³	113.5	114.1	1509.7
B³–OB³–CT	109.7		1459.8
OB³–CT–CT	103.5		1810.3
OB³–CT–CA	103.5		804.8
torsion angle	**phase angle ψ [deg]**	**multiplicity m**	**force constant [kJ/mol·rad²]**
CA–CA–B³–OB³	180.0	2	2.7
CA–B³–OB³–CT	0.0	1	69.3
OB³–B³-OB³–CT	180.0	1	118.1
B³–OB³–CT–C*	180.0	3	0.9

[a]C* indicates CA or CT atoms.

Figure 4. QM energy profiles (solid lines) for bond angles CA–CA–B³, CA–B³–OB³, OB³–B³–OB³, B³–OB³–CT, OB³–CT–CT, and OB³–CT–CA. Dashed lines represent the fit of the QM data by a harmonic potential as described in eq 1.

The atoms B³ and OB³ are involved in six bond angles: CA–CA–B³, CA–B³–OB³, OB³–B³–OB³, B³–OB³–CT, OB³–CT–CT, and OB³–CT–CA. The equilibrium values of these bond angles are listed in Table 4. We also compared the values of the computed angles with the corresponding experimental values. Only two angles are available from the *MANBOS* crystal structure, i.e., CA–B³–OB³(123.0°) and OB³–B³–OB³(114.1°), with a good agreement between QM calculations and X-ray experiments (Table 4).

Torsion Angle Parameters. To maintain consistency with the existing AMBER force field, torsion angle parameters for atom types that already existed in the force field were not
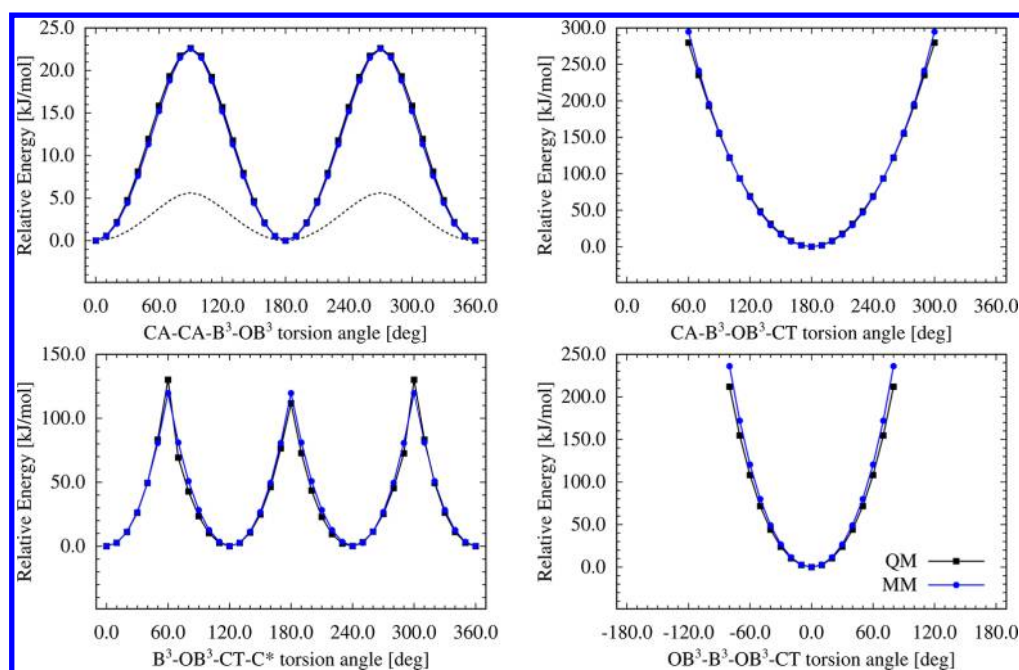
Figure 5. QM (black) and MM (blue) energy profiles for torsion angles CA−CA−B³−OB³, CA−B³−OB³−CT, B³−OB³−CT−C* (C* = CA or CT), and OB³−B³−OB³−CT. Dashed lines represent MM energy profiles before any adjustment (see text).

optimized, i.e., rotations around CA−CA, CA−CT, and CT−CT bonds. As described in a previous section, three bonds contain B³ and OB³ atoms, i.e., CA−B³, B³−OB³, and OB³−CT, which means that rotations about these three bonds must be parametrized to describe accurately the torsion dynamics of GOF materials. This corresponds to four torsion angles: CA−CA−B³−OB³ for the rotation around CA−B³ bond, CA−B³−OB³−CT and OB³−B³−OB³−CT for rotations around B³−OB³ bond and B³−OB³−CT−C* (C* = CA or CT) for the rotation around the OB³−CT bond (Table 4). In addition, as shown in eq 1, the potential describing these rotations is a periodic potential, which means that, contrary to bond lengths and angles described by harmonic potentials, we have to explore the complete energy profiles of each torsion angle to determine the phase and the associated multiplicity. The corresponding energy profiles are shown in Figure 5. The overall energy profiles for torsion angles are significantly influenced by Coulombic and van der Waals interactions of the atoms involved in each torsion angle, and consequently, we decided to adjust QM energy profiles of torsion angles to reproduce their corresponding MM energy profiles. Although MM torsion angle energy profiles reproduced the shape of the QM energy profiles, energy barrier heights are much lower (Figure 5, top left panel). Therefore, the force constants K_ϕ for each torsion angle, which have been estimated from QM energy profiles, were optimized to reproduce their corresponding MM energy profiles.

The CA−CA−B³−OB³ torsion angle corresponds to the rotation of the phenyl ring around the CA−B³ bond and can be described by a periodic potential with a phase angle $\psi = 0°$ and a multiplicity $m = 2$, due to the symmetry of the phenyl ring (Figure 1B). The positions $\phi = 0°$ and $180°$ are equivalent by symmetry and correspond to the two most stable positions. The angles $\phi = 90°$ and $270°$ correspond to a phenyl ring perpendicular to the trigonal boronic acid plane (Figure 1B) and are the least stable positions. The CA−B³−OB³−CT torsion angle characterizes the height of the phenyl ring with respect to the graphene sheet in the PBA model fragment shown in Figure 1B. It is described by a periodic potential with a phase angle $\psi = 180°$ and a multiplicity $m = 1$. A phase angle $\psi = 180°$ corresponds to the maximum height between the phenyl ring and the graphene sheet. We have not plotted, in Figure 5, the potential of this torsion angle for $60°$ and $\phi > 300°$ since these angles correspond to very short distances between he phenyl ring and graphene and yield high potential energy values. The B³−OB³−CT−CT and B³−OB³−CT−CA are equivalent torsion angles due to the sp³ hybridization of CT atoms (tetrahedral arrangement; see Figure 1), which is characterized by a periodic potential with a phase angle $\psi = 0°$ and multiplicity $m = 3$ for B³−OB³−CT−C* torsion angles (Table 4). Finally, the OB³−B³−OB³−CT torsion angle, which represents the plane of the pentagon formed by atoms B³, OB³, and CT atoms is modeled by a periodic potential with a phase angle $\psi = 0°$ and a multiplicity $m = 1$. This very deep torsion potential is not plotted in Figure 5 for $\phi < −80°$ and $\phi > 80°$ since these angles yield very high energy values. At these angles, the linker is no longer bonded to the graphene sheet, i.e., OB³−CT bonds are broken.

Validation of the Force Field Parameters. As the final stage of the parametrization procedure, we now test the validity of the parameters without any further adjustment (Tables 3 and 4) by comparing two different QM and MM properties.

MM vs QM: Geometry Optimization. First, we tested the validity of the parameters by comparing structures obtained from QM geometry optimization and MM energy minimization. This comparison is quantified by computing the root-mean-square deviation (RMSD):

$$\text{RMSD}(r^{QM}, r^{MM}) = \sqrt{\frac{1}{N_{atom}} \sum_i \|r_i^{QM} - r_i^{MM}\|^2} \tag{3}$$

where $r_i(QM)$ and $r_i(MM)$ denote the position of an equivalent atom i in the QM and MM optimized structure and N_{atom} is the total number of atoms. The first test structure is the PBA model

fragment shown in Figure 6A. The RMSD(r^{QM}, r^{MM}) is equal to 0.005 nm, indicating that the parameters reproduce faithfully
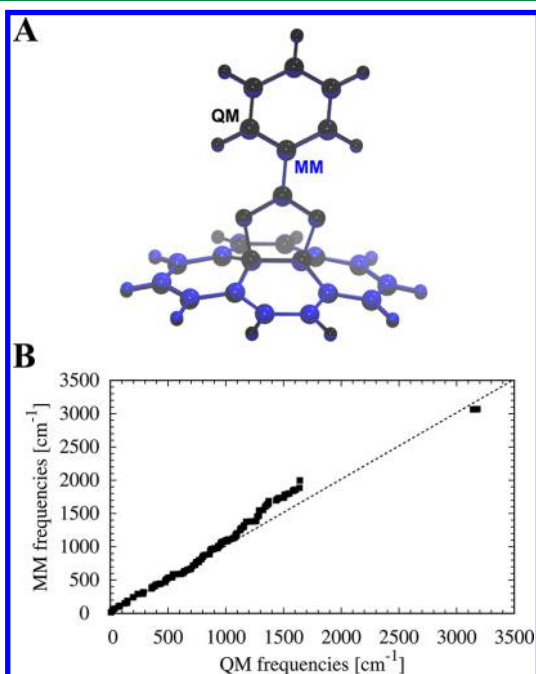
Figure 6. [A] Comparison of 3D all-atom structures obtained from QM (black) and MM (blue) geometry optimizations. The alignment of the two structures was done by minimizing the RMSD between all the atoms. [B] Vibrational frequencies of the PBA model fragment shown in Figure 1B. The dashed line shows the ideal fit between QM and MM data.

the QM geometry optimization (Figure 6A). We also used the GOF-L-32 structure to assess the transferability of MM parameters from the PBA model fragment (Figure 1B) to GOF materials (Figure 1A). The RMSD(r^{QM}, r^{MM}) is equal to 0.007 nm (structures not shown), thereby confirming the excellent transferability and the relevance of the new parameters for structural analysis of GOF materials using MD simulations.

MM vs QM: Vibrational Frequencies. Second, we compared the QM and MM vibrational frequencies of the QM and MM optimized PBA model fragments shown in Figure 6A. The resulting plot of ω^{QM} and ω^{MM} is shown in Figure 6B. In this plot, the closer to the diagonal the points, the better the fit. Up to 1000 cm^{-1}, the agreement between QM and MM vibrational frequencies is very good. This range of frequencies contains the "slow" collective modes of the structure, which correspond to

the largest fluctuations of the system and are of particular interest in MD simulations. However, we also note a deviation for modes with higher frequencies corresponding to small fluctuations, leading to an RMSD(ω^{QM}, ω^{MM}) = 128.5 cm^{-1}. Of course, one cannot expect a perfect match between QM and MM vibrational frequencies ω in the high frequency range. As mentioned above, we are interested in the structural flexibility of GOF materials using MD simulations, which correspond to large fluctuations. Therefore the observed deviation for high frequencies, which characterized small fluctuations like bond stretching for example, has little impact within the scope of applicability as research presented in the present work.

MD Simulations of GOF Materials. As a full MD application of the new parametrization for GOF materials, we chose to investigate the dynamical behavior of GOFs in explicit solvent for five distinct types of GOF materials with varying linker density: GOF-L-16, GOF-L-32, GOF-L-64, GOF-L-128, and GOF-∞ with L = 44BPDBA (Figure 7). We performed all-atom unbiased MD simulations of each GOF-L-n material in explicit water using the TIP3P[17] water model in the NPT ensemble (N is given in Table 2, P_0 = 1 bar, and T = 300 K) during 20 ns.

Structural Flexibility of GOF Materials. To characterize the structural properties of GOF materials during MD simulations in explicit solvent, we computed the RMSD of GOF-L-n materials as a function of time t using the initial frame at $t = t_0$ as a reference, i.e., we computed RMSD($r(t)$, $r(t_0)$) for each MD run according to eq 3. The alignment of the different structures was performed using all the atoms of GOF-L-n. As shown in Figure 8A, the structure of GOF-L-n is very stable during MD simulation and only fluctuates around its equilibrium position. On average, the RMSD for GOF-L-32 during its 20 ns MD run is 0.021 nm, with similar values obtained for the other GOF-L-n (data not shown). Moreover, the most flexible part of GOF-L-n materials is the linker, and particularly the phenyl rings, as shown in Figure 8B. This can be seen from a plot of the root-mean-square fluctuations (RMSF), which measures the average atomic mobility during MD simulations:

$$\text{RMSF}_i = \sqrt{\frac{1}{N_{\text{time}}} \sum_t \|r_i(t) - \langle r_i \rangle\|^2} \quad (4)$$

where N_{time} is the production time of MD simulations and $\langle r_i \rangle$ is the average position of atom i. Note that the difference between the information included in RMSD and RMSF is that while the latter implements averages over time (N_{time}), yielding a different value for each atom i, for RMSD, the average is run over the particles (N_{atom}), at a given time value t. The RMSF
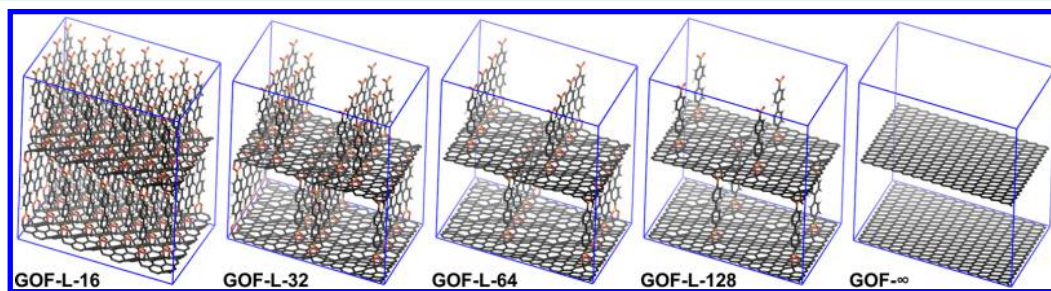
Figure 7. 3D all-atom periodic structures of idealized GOF-L-n materials used as initial structures in MD simulations (L = 44BPDBA and n = 16, 32, 64, 128, and ∞). The color code is the same as in Figure 1. The simulation boxes are represented by blue lines.
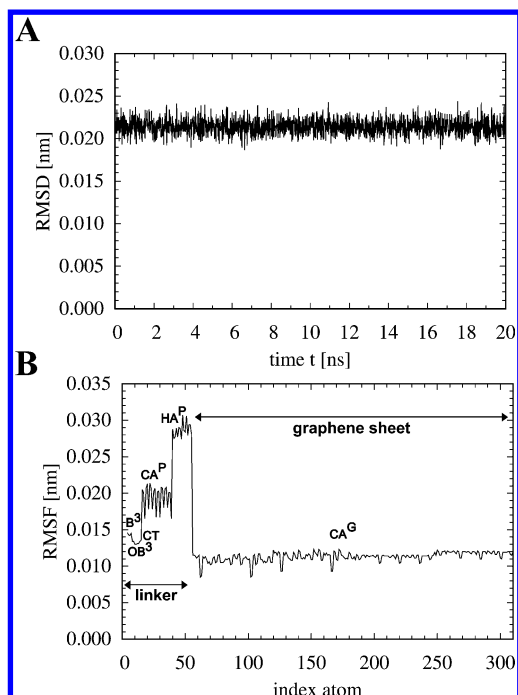
Figure 8. [A] RMSD$(r(t), r(t_0))$ of GOF-L-32 as a function of time t with respect to the initial frame t_0. Only every 100 ps time steps are represented for more clarity. [B] RMSF$_i$ of GOF-L-32 computed from 0 to 20 ns. Only a periodic fragment of the full GOF structure is represented.

(Figure 8B) indicates a high flexibility for aromatic hydrogen HA and aromatic carbon CA atoms of the phenyl rings, whereas the carbon atoms of the graphene sheet are very rigid. CT atoms, which represent the linkage between the pillar units and the graphene sheet are also rigid, as well as B^3 and OB^3 atoms. The flexibility of the linker, compared to the rigidity of the graphene sheet, can be explained by the diffusion of water inside the GOF materials and the close proximity between water molecules and linkers whereas, due to its hydrophobicity, graphene sheets are not in close contact with water molecules and the mobility effect of water molecules is weak.[24,25] Similar to RMSDs, the same RMSF behavior is observed for other GOF-L-n materials, independent of the density of linkers $1/n$ (data not shown).

Dynamical and Structural Properties of Water Inside GOFs. The diffusion properties of water inside GOF-L-n materials have been analyzed by computing the mean-square displacement (MSD) of the water molecules' center of mass. From such an analysis, one can characterize the diffusion mechanism and calculate the self-diffusion coefficient of water molecules using the following equation:

$$\text{MSD}(t) = \langle |(r(t) - r(0))|^2 \rangle = 2dDt^\alpha \tag{5}$$

where r denotes the center of mass coordinate of the water molecules; the angle bracket defines the average over all the water molecules; t is the time interval; D is the self-diffusion coefficient; d is the dimensionality of the system ($d = 3$ in our study); and α defines the type of diffusion mechanism.[26]

Depending on the temporal variation of MSD, different diffusion mechanisms can be identified based on the parameter α and the power law of the MSD as a function of time; i.e., $\alpha =$
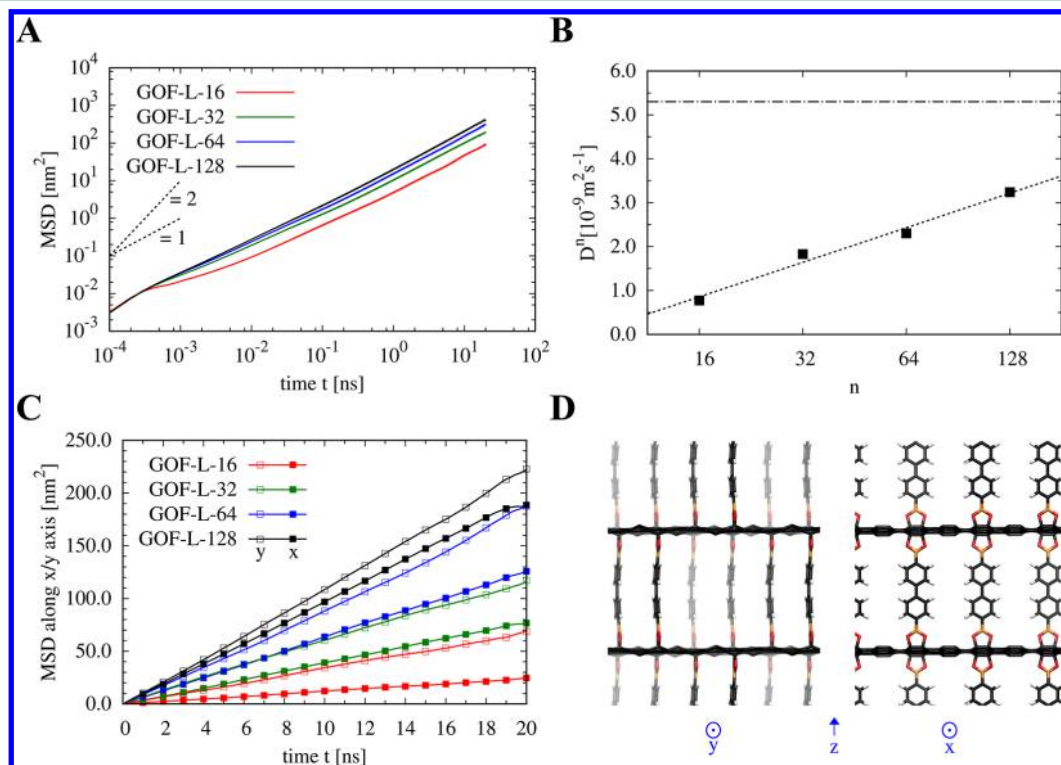
Figure 9. [A] MSD of water molecules as a function of the density of linkers $1/n$. Dashed lines represent linear curve with slopes of 1 and 2. [B] Diffusion coeffcient D^n computed from MSD curves between 100 ps and 10 ns as a function of the density of linkers $1/n$. The dashed−dotted line represents the diffusion coefficient of bulk water. [C] MSD of water molecules in x (empty squares) and y (filled squared) directions as a function of the density of linkers $1/n$. [D] 3D all-atom initial structures of GOF-L-32 showing the x and y directions. The color code is the same as in Figure 1A.
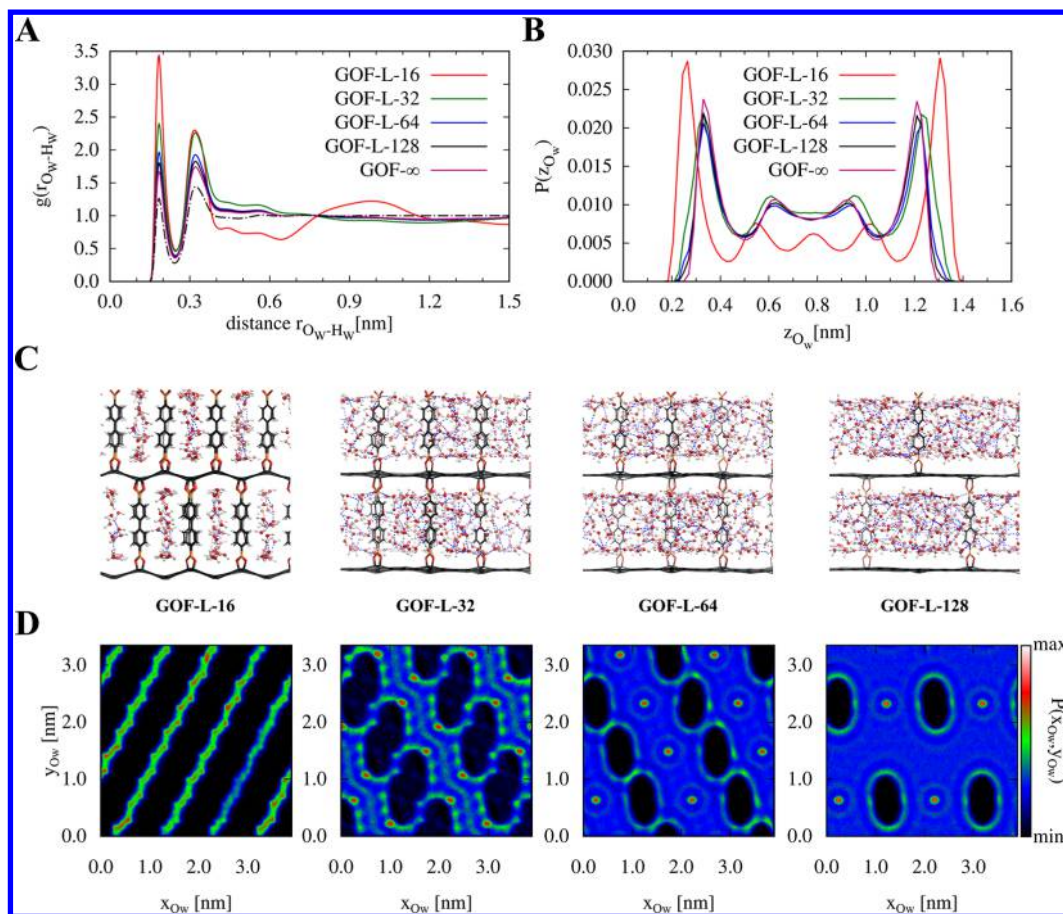
Figure 10. [A] RDF of oxygen−hydrogen (Ow−Hw) atoms of water molecules $g(r_{Ow-Hw})$ as a function of the density of linkers $1/n$. The dashed−dotted line represents the diffusion coefficient of bulk water. [B] PDF of z coordinates of oxygen (Ow) atoms of water molecules $P(z_{Ow})$ as a function of the density of linkers $1/n$. [C] 3D all-atom structures of snapshots (20 ns) at the end of MD runs for GOF-L-16, 32, 64, and 128 in interaction with water molecules. The color code is the same as in Figure 1A. Dashed blue lines represent hydrogen bonds (cutoff = 0.3 nm). [D] 2D PDF of (x,y) coordinates of oxygen (Ow) atoms of water molecules $P(x_{Ow}, y_{Ow})$ as a function of the density of linkers $1/n$. The black color represents a probability $P(x_{Ow}, y_{Ow})$ equal to zero, and the red one, the maximum probability.

0.5 refers to single-file diffusion, $\alpha = 1$ refers to the Fickian diffusion, and $\alpha = 2$ refers to ballistic diffusion.[26] As shown in Figure 9A, MSDs of water molecules inside GOF-L-n materials increase linearly as a function of time after a few picoseconds, i.e., $\alpha = 1$ (Fickian diffusion). A ballistic diffusion ($\alpha = 2$) is observed from the beginning of the MD runs to a few picoseconds, due to the equilibration of the system after the generation of initial velocities at $t = 0$. Self-diffusion coefficients D^n were then calculated from MSD curves from 100 ps to 10 ns. As expected, the diffusion coefficients of water molecules are reduced when the number of carbon atoms of the graphene sheet n per linker decreases, i.e., when the density of linker $1/n$ increases (Figure 9B) and are smaller than the self-diffusion coefficient D of bulk water (Figure 9B).

The diffusion coefficients of water molecules increase linearly with n, as shown in Figure 9B, indicating that the linker density could be varied (as done experimentally[2]) to tune the diffusion properties of GOF-L-n. The effect of the density of linkers on the dynamical properties of water molecules inside GOF-L-n materials can be further investigated by analyzing the in-plane diffusion of water molecules (xy-plane). Different densities of linkers for a given type of linker L in GOF-L-n materials involve structural differences in the xy plane whereas different linkers L for the same linker density involve structural differences in the xz plane. As shown in Figure 9C, the mobility of water molecules is larger in the y direction than in the x direction, regardless the value of the linker density. This difference in mobility is due to the orientation of the linkers in GOF structures (Figure 9D). GOF linkers L belong to the yz plane, which means that the mobility of water molecules in the y direction (Figure 9D) is not affected by phenyl rings of linkers compared to the x direction, which slow down the diffusion of water molecules (Figure 9D). Moreover, the difference in the mobility of water molecules between the x and y directions for GOF-L-128 is less important due to the very low density of linkers which allows water molecules to diffuse more easily between linkers.

This is not the case for the other GOF-L-n, with $n < 128$, because the linkers are much closer (Figure 7). Hence, the resulting hydrogen-bonding network between water molecules can be significantly different depending on n. Radial distribution functions (RDFs) between oxygen and hydrogen atom pairs of water molecules (Ow−Hw) can be used to identify hydrogen-bonding network characteristics of these confined water molecules. The RDF $g(r)$ is defined as the probability of finding an atom type 1 at a distance r from another atom type 2 compared to a homogeneous distribution:[26]

$$g(r) = \frac{V}{N_1 N_2} \frac{1}{4\pi r^2 \delta r} \left\langle \sum_i \sum_{j>i} \delta(r - r_{ij}) \right\rangle \quad (6)$$

where V is the volume and N_k is the number of atoms of type k. Figure 10A shows the radial distribution function for oxygen−hydrogen (Ow−Hw) atom pairs of water molecules, $g(r_{Ow-Hw})$, inside GOF-L-n for various n. The first nearest neighbor distance in Ow−Hw RDFs, i.e., 0.184 nm, corresponds to the intramolecular bonds of water molecules and is not affected by the linker density since it is defined by the TIP3P water model.[17] The second peak of RDFs, at 0.314 nm, represents the intermolecular hydrogen-bonding network of water molecules observed during MD simulations of GOF-L-n and is not affected by the density of linkers either. This second peak corresponds to the first shell of water molecules. These two first peaks are also observed for bulk water RDF $g(r_{Ow-Hw})$. Notably, GOF-L-16 shows a different behavior for larger Ow−Hw distances compared with the other GOF-L-n materials: the large bump between 0.8 and 1.2 nm is not present for GOF-L-n materials with $n > 16$ (Figure 10A). In addition, GOF-L-n materials with $n > 32$ show a similar behavior as GOF-∞. The RDFs $g(r_{Ow-Hw})$ of these three systems are almost identical (Figure 10A); the density of linkers is so slow that water molecules confined in GOFs are not fully disturbed by the presence of linkers and these systems could be assimilate to graphene sheets without linkers.

To understand the origin of this difference, we first examined the probability distribution function (PDF) of z coordinates of Ow atoms, $P(z_{Ow})$, between two graphene sheets. As shown in Figure 10B, two major peaks are observed, corresponding to confined water near the graphene sheet interfaces, at a distance of 0.3 nm for GOF-L-16 and 0.35 nm for the other GOF materials. Note that it is not surprising that the shape of the PDF $P(z_{Ow})$ does not depend on the density of linkers, since the linkers are identical. It is also confirmed by the PDF $P(z_{Ow})$ of GOF-∞, which shows exactly the same trends as observed for the other GOF-L-n materials. This peak is shifted by 0.05 nm between GOF-L-16 and the other GOF materials. This can be explained by the fact that, in the case of GOF-L-16, the graphene sheets are not planar (Figure 10C). The corresponding curvature, which is only observed in GOF-L-16 materials from MD simulations and previously from DFT calculations,[4] is due to the presence of a large number of linkers and consequently of CT atoms (sp^3 carbon atoms with tetrahedron geometries) in the graphene sheets. Therefore water molecules are allowed to diffuse in a larger range of z values. In addition, it involves the appearance of a small peak in $P(z_{Ow})$ at 0.8 nm for GOF-L-16.

To explain the presence of the large bump between 0.8 and 1.2 nm in the RDF $g(r_{Ow-Hw})$ of GOF-L-16, we examined the structure of water inside GOF materials (Figure 10C). It appears that water molecules inside GOF-L-16 are confined in independent channels, whereas they can diffuse from a channel to another one for $n > 16$. This phenomenon is confirmed by the in-plane (xy) trajectory of the water molecules. Indeed, as shown above, the difference of linker density involves an n-dependent in-plane (xy) diffusive behavior (Figure 9C).

To characterize this behavior, we plotted the 2D-PDFs $P(x_{Ow}, y_{Ow})$ of oxygen atoms of water molecules between two graphene sheets, as shown in Figure 10D. The 3D structure of water inside GOF-L-16 (Figure 10C), the 2D-PDF $P(x_{Ow}, y_{Ow})$ confirms that water molecules diffuse in independent channels and no exchange takes place between these narrow channels. In

addition, the width of these independent channels is around 1.0 nm, indicating that the large bump between 0.8 and 1.2 nm observed in the RDF of water molecules $g(r_{Ow-Hw})$ in GOF-L-16 corresponds to the distance between water clusters in two neighboring channels.

For $n > 16$, water molecules also diffuse in channels but they are no longer independent. As shown in Figure 10D, the probability for a water molecule to cross over from one channel to another is not zero. Moreover, the channels become larger as n increases and the exchange rate becomes gradually more important. For $n > 32$, the channels are so large than the behavior of water molecules confined in GOF-L-n is quite similar to the behavior of the same molecules between independnt graphene sheets, as is the case of GOF-∞. Finally, the probability to find a water molecule close to a linker becomes significant due to the presence of donors and acceptors HA^P and OB^3 atoms in the 4,4′-biphenyldiboronic acid linkers and the possibility of an hydrogen-bonding network between water molecules and linkers L.

CONCLUSIONS

While only a few boron-related compounds have been studied by MD simulations, the need for a more complete set of MM force field parameters has increased with the development of new nanolayered materials, such as graphene oxide frameworks. Here, we established a MM force field parametrization for a phenylboronic acid model fragment extracted from GOF materials. This model fragment is comprised of the typical CT, CA, and HA atoms, as well as of B^3 and OB^3 atoms, for which MM parameters were missing in commonly used force fields. We also developed a new set of bonded and nonbonded parameters of a PBA model fragment, which is compatible with the AMBER potential energy surface. The parametrization is based on reproducing quantum-mechanically derived target data and validated by comparing QM and MM structural and vibrational properties. The parametrization was used to study the dynamics of GOF materials filled with water molecules.

We considered idealized GOF-L-n materials (Figure 1A), where L stands for 4,4′-biphenyldiboronic acid linker (L = 44BPDBA) and n stands for n graphene sheet carbons per linker unit. The influence of the density of linkers on the diffusion properties of water molecules inside GOF materials was examined. The results show that the diffusion mechanism of water molecules inside GOF-L-n materials is a Fickian type of diffusion and that self-diffusion coefficients D^n of water molecules increase linearly with n. This result indicates that one should be able to tune the diffusion properties of GOF materials by modifying the density of linkers. In addition, by studying the flow of water molecules inside GOF materials, we showed that GOF-L-16 materials are characterized by very narrow, independent channels, which involves a quasi-one-dimensional diffusion of water molecules inside these channels (Figure 10D). Indeed, water molecules are confined between graphene sheets in the z direction, as in the other GOF materials, but also in x and y directions due to the density of the linkers. When n increases, channels can communicate and a water flow is established between these channels. Similar to the diffusion coefficient, the width and the exchange rate of water molecules between the channels are a tunable function of the density of linkers.

AUTHOR INFORMATION

Corresponding Author

*E-mail: meuniv@rpi.edu. Phone: (518) 276-6886. Fax: (518) 276-668.

Notes

The authors declare no competing financial interest.

REFERENCES

(1) Burress, J. W.; Gadipelli, S.; Ford, J.; Simmons, J. M.; Zhou, W.; Yildirim, T. *Angew. Chem., Int. Ed.* **2010**, *49*, 8902−8904.

(2) Srinivas, G.; Burress, J. W.; Ford, J.; Yildirim, T. *J. Mater. Chem.* **2011**, *21*, 11323−11329.

(3) Chan, Y.; Hill, J. M. *Nanotechnology* **2011**, *22*, 305403 PMID: 21719967.

(4) Zhu, P.; Sumpter, B. G.; Meunier, V. *J. Phys. Chem. C* **2013**, *117*, 8276−8281.

(5) Tafi, A.; Agamennone, M.; Tortorella, P.; Alcaro, S.; Gallina, C.; Botta, M. *Eur. J. Med. Chem.* **2005**, *40*, 1134−1142.

(6) Otkidach, D.; Pletnev, I. *J. Mol. Struct.: THEOCHEM* **2001**, *536*, 65−72.

(7) Chen, X.; Bartolotti, L.; Ishaq, K.; Tropsha, A. *J. Comput. Chem.* **1994**, *15*, 333−345.

(8) Weiner, P. K.; Kollman, P. A. *J. Comput. Chem.* **1981**, *2*, 287−303.

(9) Bayly, C. I.; Cieplak, P.; Cornell, W.; Kollman, P. A. *J. Phys. Chem.* **1993**, *97*, 10269−10280.

(10) Wang, J.; Cieplak, P.; Kollman, P. A. *J. Comput. Chem.* **2000**, *21*, 1049−1074.

(11) Berendsen, H.; van der Spoel, D.; van Drunen, R. *Comput. Phys. Commun.* **1995**, *91*, 43−56.

(12) Valiev, M.; Bylaska, E.; Govind, N.; Kowalski, K.; Straatsma, T.; Van Dam, H.; Wang, D.; Nieplocha, J.; Apra, E.; Windus, T.; de Jong, W. *Comput. Phys. Commun.* **2010**, *181*, 1477−1489.

(13) Becke, A. D. *J. Chem. Phys.* **1993**, *98*, 5648−5652.

(14) Stephens, P. J.; Devlin, F. J.; Chabalowski, C. F.; Frisch, M. J. *J. Phys. Chem.* **1994**, *98*, 11623−11627.

(15) Dunning, T. H. *J. Chem. Phys.* **1989**, *90*, 1007−1023.

(16) van der Spoel, D.; Lindhal, E.; Hess, B.; van Buuren, A. R.; Apol, E.; Meulenhoff, P. J.; Tielemann, D. P.; Sijbers, A. L. T. M.; Feenstra, K. A.; van Drunen, R.; Berendsen, H. J. C. *Gromacs User Manual version 4.5.5*, 2011; www.gromacs.org (accessed March 2013).

(17) Jorgensen, W. L.; Chandrasekhar, J.; Madura, J. D.; Impey, R. W.; Klein, M. L. *J. Chem. Phys.* **1983**, *79*, 926−935.

(18) Nosé, S. *J. Chem. Phys.* **1984**, *81*, 511−519.

(19) Hoover, W. G. *Phys. Rev. A* **1985**, *31*, 1695−1697.

(20) Parrinello, M.; Rahman, A. *J. Appl. Phys.* **1981**, *52*, 7182−7190.

(21) Darden, T.; York, D.; Pedersen, L. *J. Chem. Phys.* **1993**, *98*, 10089−10092.

(22) Hess, B.; Bekker, H.; Berendsen, H. J. C.; Fraaije, J. G. E. M. *J. Comput. Chem.* **1997**, *18*, 1463−1472.

(23) Allen, F. H. *Acta Crystallogr., Sect. B: Struct. Sci.* **2002**, *58*, 380−388.

(24) Leenaerts, O.; Partoens, B.; Peeters, F. M. *Phys. Rev. B* **2009**, *79*, 235440.

(25) Wang, S.; Zhang, Y.; Abidi, N.; Cabrales, L. *Langmuir* **2009**, *25*, 11078−11081.

(26) Allen, M. P.; Tildesley, D. J. *Computer Simulation of Liquids*; Oxford University Press: New York, 1989; pp 182−208.